This document is the accepted manuscript version of the following article:
Adams, D. J., Chappellet, S., Lincker, F., Ibn-Elhaj, M., Watts, B., Iannuzzi, M., … Passerone, D. (2014). Identifying photoreaction products in cinnamate-based photoalignment materials. Journal of Physical Chemistry C, 118(28), 15422-15433. https://doi.org/10.1021/jp504765f

Identifying Photoreaction Products in Cinnamate Based Photoalignment Materials

*Donat J. Adams[1], Sabrina Chappellet[2], Frédéric Lincker[2], Mohammed Ibn-Elhaj[*2], Benjamin Watts[3], Marcella Iannuzzi[4], Dubravka Šišak Jung[5,†], Carlo A. Pignedoli[1],* and *Daniele Passerone[*1]*

[1]Empa, Swiss Federal Laboratories for Materials Science and Technology, nanotech@surfaces Laboratory, Dübendorf (Switzerland); [2]Rolic Technologies Ltd, Allschwil, Switzerland; [3]Swiss Light Source, Paul Scherrer Institute, Villigen-PSI (Switzerland); [4]University of Zurich, Institute of Physical Chemistry, Zurich (Switzerland); [5]Laboratory of Crystallography, Department of Materials, ETH Zurich, Zurich (Switzerland).
E-mail: daniele.passerone@empa.ch

Keywords: Photoalignment materials, NEXAFS, infrared spectroscopy, ab initio simulation

ABSTRACT. A novel joint computational and experimental strategy is developed and applied for the detection and the identification of photoreaction products in cinnamate based photoalignment materials. Based on NEXAFS, IR, and NMR spectroscopies and supported by computer simulation tools, this structural analysis method allows distinguishing the typical signatures of products resulting from UV-induced photoreactions between isomers of cinnamate based model compounds. Besides deepening the understanding of typical photoalignment reaction products, the proposed strategy acquires technological relevance in supporting the realization of next generation materials for the LCD panel industry.

1. Introduction

Homogeneous and stable alignment of liquid crystal (LC) molecules is a key technology in the development of high efficiency and novel liquid crystal displays (LCDs). Until recently, conventional alignment methods such as the rubbing of polyimide layers or geometrical patterning (such as topologies or protrusion) via photo-lithographic processing were the methods of choice for large-scale production of LCDs. However, the rubbing of polyimide generates dust, static electricity and mechanical damage, which lower the yield and performances of LCDs. Also, micro-topologies reduce LCD performances such as light transmission and response time [1]. Moreover, obtaining multi-domains with different LC orientations, to improve viewing angles, requires complicated and costly processing and reduces yield. Over the past 20 years, the development of alternative LC alignment methods to overcome problems associated with rubbing has been a great challenge for the flat panel industry especially for cost-effective production of large panel LCDs with improved viewing angles.

One of the most attractive alternatives is the photo- or optical alignment process, which makes use of linearly polarized ultraviolet (UV) light to generate anisotropic alignment films. Three fundamentally different aligning strategies by linearly polarized light have been pursued, namely (i) optically induced cis-trans isomerisation of azo-based single-chromophores [2-5], (ii) photo-degradation or photo-rubbing of polyimide layers [6] and (iii) photo-alignment with cross-linkable materials [7]. So far, the first two methods suffer either from stability, yield and/or limited LCD performances [5,8,9].

Because of in-situ photo crosslinking during processing [7,10], Rolic photoalignment LCMO (Light Controlled Molecular Orientation) technology is inherently thermally and optically stable. This renders LCMO the breakthrough alignment technology for todays advanced mass-production for large LCD-TV panel and 3D converters. This fundamental technology allows an easy achievement of high resolution azimuthal LC-director patterns with defined bias tilt angles, from homogeneous planar to vertical alignment (VA), depending on the target application [7,10-15]. Among others, this technology is actually used in the manufacturing of advanced large LCD-TV VA-panel displays with reduced production costs and low energy consumption [1,16], as well as roll-to-roll mass-production of state of the art 3D converter films for 3D-displays such as the film patterned retarders (FPR) manufactured by LG.

The key process in LCMO photoalignment is the UV-light induced chemical reaction between side chains of neighboring polymers or within the polymer itself.

The photo-sensitivity, the photo-reactions involved, as well as the resulting alignment and LCD performances depend strongly on the chemical structure of the material. **Fig. 1** (left inset) shows the base molecular structure of a typical Rolic alignment material, based on a photoreactive cinnamate fragment. The different chemical groups of this complex system are responsible for alignment control, alignment homogeneity, pre-tilt and film stability as well as other required electrical- and electro-optical performances. The development of state of the art industrial materials is, so far, based on long-term empirical expertise and chemical design capabilities.

Experimentally, trans-cis transformation and formation of dimers have already been observed long time ago in cinnamate-based liquid, glass and solid phases [17,18]. The photochemical reactions

which occur upon exposure of cinnamate based polymers to unpolarised light [19] have been analytically investigated for some classical photopolymers such as poly(vinylcinnamate) (PVCin). The existence of cyclic products in unpolarised-UV irradiated PVCin polymer films has been clearly established. However, cycloaddition should not be the only photoprocess occurring in PVCin, especially in solutions. In solid PVCin films though, it was found that isomerisation plays only a minor role and does not seriously interfere with cyclization or any other bimolecular photoprocess [19]. Linear polymerisation was reported to arise from thermal crosslinking [20].

A better understanding of this system should disclose systematic improvement of the materials and support development of next generation technology and photo-alignment materials. The very complex nature of the problem, however, does not allow a full description of this process. Therefore, in the present paper we focus on the polymer photoreactive side chains and report on a joint experimental and theoretical effort based on a model compound representative of such chains. We aim to understand and identify signatures of its structural and chemical modifications induced by photoradiation. We first synthesize molecular samples of a cinnamate derivative (ethyl 4-hydroxycinnamate). With a chemical procedure we are able to isolate isomerically pure Cis and Trans forms that we analyze using infrared (IR) and nuclear magnetic resonance (NMR) spectroscopy. We then produce thin films of such molecules, and perform a near-edge x-ray absorption fine structure (NEXAFS) spectroscopic analysis of the films. The same procedure is repeated with UV-irradiated samples. The experiments are complemented by density functional theory calculations that allow to rationalize the observed properties and to connect them to structural and electronic modifications of specific molecular fragments.

Our experimental and theoretical results show that NEXAFS experiments might even allow to distinguish isomers of a single 4-hydroxycinnamate molecule and that a combined approach using NEXAFS and IR data allows even to discriminate most of the 11 dimers that can form upon UV irradiation. Finally we find that NMR can confirm the results for NEXAFS and IR but also allows to distinguish dimerization from crosslinking. Such combination of different techniques and approaches (theoretical and experimental) on controlled model systems is proposed as a strategy for analyzing the effect of UV irradiation on more complex systems involving side chains based on the cinnamate unit, like those employed in the production of state of the art thin alignment films in the LCD industry.

2. Choice of the model system

As indicated in **Fig. 1 (left inset)**, typical base polymers used in final products consist of a polymer backbone, generally of acrylate or polyimide type, and a side-chain chromophore comprising a simple cinnamic acid photoactive group linked on both sides to different functional groups that can lead to complex side-chain structures.

In the LCMO polymer films, in addition to the cycloaddition reactions, UV light can either induce isomerizations of such side chains or reactions between them that can cause cross-linking of two or more side chains. In order to control the alignment properties and stability of the polymer film by the proper choice of side chains and experimental conditions, it is important to predict and understand which reaction channels (see **Fig. 1**) are more likely and how to distinguish different kinds of products by experiment.

Here, ethyl 4-hydroxycinnamate, which is the basic photo-reactive group in typical LCMO polymers, was selected as the model molecule in order to determine the signatures of compounds

that could result from the photoreaction. **Fig. 1** shows the main three different products which could be obtained after the UV-Exposure or thermal treatment process of *trans*-cinnamate (Trans); i.e. the *cis*-cinnamate (Cis) resulting from photo-isomerisation, the cyclobutane Dimer following a photocycloaddition of two Trans molecules, and a linear cross-linked complex.

3. Cis and Trans model molecule characterization

3.1 Structure from ab initio simulations

The model molecules (Cis and Trans) were optimized in the gas phase at the density functional theory (DFT) level using the Perdew-Burke-Ernzerhof (PBE) exchange and correlation functional. The optimized structures are shown in **Fig. 1 (right inset)**. The UV-active bond is the double bond between carbons **C1** and **C2** (bond length: 1.35 Å). The torsion angle involving this bond is 180.2° for the Trans, and 18.5°for the Cis. This angle characterizes the isomers.

We plot in **Fig. 2** the frontier orbitals for the two cases. The HOMO-LUMO gap is found to be 3.3 eV (2.8 eV for the cis) . We note that at the PBE level an underestimation of the gap is expected. Using the B3LYP hybrid functional we find orbitals of similar shape, but with an HOMO-LUMO gap amounting to 4.7 eV (4.2 eV for the cis).

The electric dipole moment of the two model molecules was found to be 2.24 Debye and 2.70 Debye for the Trans and the Cis respectively. The orientation is along the molecular axis in the Trans case and orthogonal to it in the Cis case.

3.2 Experimental and theoretical characterization by IR spectroscopy.

The infrared (IR) spectra of the Cis and Trans are shown in **Fig. 3**, blue line. We focus here on the vibrations involving the vinylene double bond C=C of the cinnamoyl moiety. The most

characteristic IR vibrations of this kind are in the 1800 – 800 cm^{-1} spectral range. Such bands of the Cis and Trans model molecule are summarized in **Table 1** together with comparison to simulation.

For a better understanding of the observed variations upon isomerization, we computed the vibrational spectrum using the harmonic approximation starting from the stable optimized structures described above [21].

The strong intensity observed in the Trans configuration at 1118 cm^{-1} is due to a collective deformation mode of CH bonds of the vinylene units and of the aromatic ring, which is oriented parallel to the dipole moment. Such enhancement (extracted from a gas-phase calculation) is not observed in experiment due to the coated film geometry. Through the projection of the normal-modes onto subgroups of chosen atoms we can analyze the contribution of different chemical sub-units. The trans-cis isomerization has the following signature:

• The group P1 at 986 cm^{-1} can be attributed to the C-H deformation vibration of the cinnamic vinylene. It shifts by -31 cm^{-1} in the Cis configuration. In experiment, the mode appears at 979 cm^{-1} (trans, the band is not present in the cis), and there is an additional band at about 1020 cm^{-1}. The literature is not uniform about the fate of the bands in this region upon isomerization. Some authors[22] interpret their experiments as a red shift of the C-H vibration band by 100 cm^{-1} upon trans-cis isomerization. Others[23] hypotesize the disappearence of the band in the Cis state. Our simulation and experiments partially confirm this scenario. To better clarify this point, we repeated our simulation with the hybrid exchange and correlation functional and the triple-zeta aug-cc-pVTZ basis set, using the package NWCHEM (http://www.nwchem-sw.org). It is known (see, e.g., the CCCBDB database [24]) that B3LYP generally overestimates the

frequencies with respect to the PBE functional. We find indeed an almost rigid shift of all frequencies by about 50 cm^{-1}. Within this method, we obtain a C-H vibrational frequency at 1025 and 1019 cm^{-1} in the Trans and Cis, respectively. This can be connected to the experimental persistence of the band at ~1020 cm^{-1} .

• The group P2 at 1296 cm^{-1} in the Trans configuration can be associated to a rocking mode of the C-H of the cinnamic vinylene. Upon isomerization, one component of the peak shifts by 91 cm^{-1} at 1387 cm^{-1} and the contribution is turned into a scissoring mode of the hydrogens; other components can be identified (indicated by P2 arrows) in the same region in the Cis case. In experiment the mode appearing for the Trans at 1312 cm^{-1} shifts to 1397 cm^{-1} (+85 cm^{-1}) after isomerization.

• The peak P3a which corresponds to the vinylene C=C stretching vibration of the cinnamoyl group at 1622 cm^{-1} (at 1630 cm^{-1} for the Trans in experiment) shifts by -4 cm^{-1}. In the experiment there are two distinct bands, one at 1630 and the other at 1690 cm^{-1}. The highest peak in this region (P3b, at 1695 cm^{-1} in experiment) corresponds to the conjugated C=O stretching vibrations of the cinnamate unit. Its position is expected not to strongly shift upon the isomerization, as this molecular subunit is less affected. Indeed a small shift of 5 cm^{-1} is observed. (11 cm^{-1} for the experiment). In theory, we observe the two peaks at 1622 and 1680 both in the Cis and in the Trans. The intensity of the C=O stretching, however, is strongly increased in the Cis (in both theory and experiment). The vibration is orthogonal (and then less active) to the dipole moment in the Trans case.

In general, the isomerization to Cis has the tendency to lower the wave number of vibrational modes. In the Cis configuration the vibrations emerge from a relatively weak H-H interaction that is mediated by the vinylene C=C double bond. In the Trans configuration the movement of

the H atoms are relative to the heavy residuals R attached to the vinylene double bond. Such H-R interaction is not mediated by the C=C double bond and is therefore strong. Thus upon trans-cis isomerization the vibrational frequencies of the C=C double bond soften [25].

3.3 Experimental and theoretical characterization by NEXAFS Spectroscopy.

Carbon K-edge NEXAFS spectra consist of resonance peaks corresponding to X-ray absorption events involving promotion of a 1s core electron into unoccupied excited molecular orbitals.

Resonances occurring near 285 eV tend to involve transitions to the π*-orbitals of C=C double bonds and aromatic rings, while those occurring between 286 eV and 290 eV tend to involve bonding to other elements and higher energy resonances usually correspond to C-C single bonds. Theoretical calculations of NEXAFS spectra might help in the assignment of resonance peaks and the interpretation of experimental spectra. NEXAFS experiments are carried out on isomerically pure films of model molecules (Trans and Cis) and we analyzed the C K-edge according to the methodology described above. In parallel, we simulated the NEXAFS spectrum using the half-core hole scheme (see the methods section).

While NEXAFS is generally considered to be insensitive to isomerisation, subtle differences in the carbon K-edge spectra of cis- and Trans,4-polyisoprene have been observed[26] .

The limited quality of the experimental spectra of the grown films (due to sublimation of the sample material in vacuum) hinders the drawing of definitive conclusions on this point (we thus report the experimental spectra in the supplementary material), however the theoretical analysis allows examination of the electronic structure differences in the empty states of the two stereoisomers.

Fig. 4 shows the computed spectra, where the contributions related to different subunits of the molecule have been separated. The contributions from the C atoms of the phenyl ring are reported in green; the contributions from the C atoms forming the double bond are reported in blue and black; the total spectrum is the red curve.

Both spectra show a large peak — the π* peak — at around 285 eV. It is composed of contributions of the delocalized orbitals on the phenyl ring and of the orbitals of the vinylene. The Trans configuration shows a very weak resonance at 284.8 eV in experiment and analysis of the atomic contributions attributes this peak to the π*- orbitals of the vinylene. In the Cis isomer, this peak is shifted to higher energy, and we may attribute the shift to the interaction of the p orbitals in C=C with the neighboring oxygen (marked with **O1** in **Fig. 1, right inset**) that modifies the chemical environment of this bond. This interaction shifts the center of gravity of the π* peak by +0.2 eV.

An alternative hypothesis is that the increased sensitivity to isomerisation observed here comes from the conjugation of bonds along the cinnamate molecule and the associated delocalisation of the electronic states (both occupied and unoccupied), which are then more strongly affected by the shape of the molecule. Given the limited quality of the experimental spectrum, we do not dare here an overinterpretation of the measured data. Rather, we focus in the next paragraphs on the relation between electronic structure and absorption spectra. As an example of how the resolution of the theoretical spectrum into atomic contribution together with the insight into the electronic structure may help in the interpretation of NEXAFS data, we analyze a specific difference between the Trans and Cis spectra, namely the markedly different peak structure between Trans and Cis of the peak at 287.2 eV and indicated by the arrow in **Fig. 4 (left panel).** Upon decomposition in atomic contributions, we note in the Trans an enhanced component from

the vinylene bond (black line) almost correspondent with a peak originating from the remainder of the molecule (not the aromatic ring).

The PDOS of the unoccupied orbitals, as reported in the left panels of **Fig. 4 (right panel)**, show that the Trans molecule has one state at 3.4 eV above the LUMO which is predominantly attributed to orbitals localized on the C=C. This state appears to be suppressed in the Cis structure.

By inspecting the shape of the corresponding orbitals (see Fig 4), we notice that the state marked by a red ellipse, at about 3.4 eV above the LUMO, is only present in the Trans. It is conjugated along the whole molecule, and is suppressed by the bent geometry of the Cis configuration (a representation of the orbital in the Trans configuration is shown in **Fig. 4** (lower left)). Upon excitation of the core electron, the excited states change their shape due to the modified core potential. Comparing the modified excited states and inspecting the corresponding intensities, we could conclude that the peak of the vinylene in the Trans originates from the state in **Fig. 4** (right) which is similar to the LUMO of the same molecule, shown in **Fig. 2**, and is suppressed in the Cis configuration**.** Instead, the part of the peak ascribed to the remainder of the molecule originates from the LUMO itself, which is shifted as higher energies when the core hole is excited from the phenyl carbon atoms.

Up to now we used an isolated molecule model to compute NEXAFS, even though the reference system is a molecular film. To assess possible environment effects on the spectra when packing the molecules in the film, we also computed the spectra of the molecular lattice. The condensed structure has been generated from the experimental lattice constant, as obtained by X-ray diffraction (see supplementary material). The internal coordinates have been then relaxed

before the calculation of the spectra. We find that the relaxation of the molecule corresponds to only a small adjustment of the molecular conformation (see supplementary material).

Nevertheless, the position of the peaks in the pre-edge region (E<290 eV) is conserved with a precision of at least 0.2 eV and there are no significant changes in intensities. The main differences are the splitting of the π* band, that has to be induced by the crystal field, and the shift to lower energies of the structures between 288 and 291 eV. This shift is attributed to the intermolecular interaction, which leads to the delocalization of the π* orbitals, thus lowering the corresponding energy.

4. Dimers characterization

Dimers of cinnamate were produced by UV irradiation, and purified by chromatography. Since irradiation can induce a cis-trans isomerization in the sample, different diastereoisomers can be obtained. The problem arises therefore: which reaction products are more probable? An answer to this question will be relevant in a realistic polymer for liquid crystal orientation, since the dimers under study correspond to two fused side chains.

Related to the four stereocenters, there are 11 non-equivalent possibilities to form a dimer out of two cinnamate molecules (trans or cis) [25,27-28] . In order to simplify the notation, we consider the cyclobutane originated by the photoreaction and classify the dimers by the stereochemistry of the residual groups containing the phenyl ring (R_{Ph}) and the ethyl group (R_{Et}), once the central cyclobutane is turned so that the majority of the four groups point out of the plane. All possible dimer stereoisomers are shown in **Fig. 5**. The constituents of the dimer are characterized by a phenyl ring and a neighboring ethyl attached to the same side (cis), or on opposite sides (trans) of the molecule with respect to the vinylene. In the dimer two model molecules can be arranged parallel (two phenyl rings on one edge, head to head [25], or antiparallel (two phenyl rings on a

diagonal, head to tail). In analogy to the truxillic acids [27] the α-, γ-, ε-, peri- and the epi-isomers can be identified within the antiparallel configuration. They correspond to tta', cta', tta, cca and cta (configurations shown in **Fig. 5**). The 6 parallel configurations have corresponding six diastereomers of truxillic acids; two of which are "meso", and four chiral. Throughout the remainder of this article we will use an explicit naming (e.g. cis-cis/antiparallel or cca), which takes into account the isomerization of the educts (trans to cis) as well as their orientation (parallel/antiparallel).

The question arises about which of such non-equivalent possibilites are likely to form out of two cinnamate monomers. A first hint can come from the energetics of the DFT calculation. Dimers have been set up and fully optimized in DFT. It turns out that the most stable dimer is tta' (see **Fig. 5**). The further dimers are higher in energy: ttp 0.13 eV, ctp' 0.14 eV, ctp 0.28 eV, ccp 0.35 eV, cta 0.44 eV and cca 0.59 eV.

As the calculations are done for an idealized system and some effects are not yet taken into account - e.g. interaction with neighboring molecules in the polymer, role of the backbone etc. - we move to further criteria to assign the reaction products to a particular combination of model molecules in the next sections.

4.1 Characterization of dimers by IR

Due to the complexity of the dimer molecules, many peaks in the IR spectra shown in **Fig. 6** and **7** are overlapping and the assignment of individual resonance peaks is difficult. The upper end of the spectrum is especially meaningful because computational errors diminish at higher frequencies and compares more successfully with experiment (see **Fig. 8**). Indeed, lower components corresponds to "slow" vibrations of the molecule whose description is affected by

the particular environment chosen, which is different in the experiment (film geometry) and in the calculation (gas phase). The calculated infrared spectra of different dimers of cinnamate are shown in the supporting material and in **Fig. 6 and 7**. The presence of bands at 1000 cm^{-1} corresponds to a stretching mode of the cyclobutane ring[29]. The contribution of the aromatic rings remains unchanged across all the spectra (orange). Appearance of bands around 1000-1100 cm^{-1} could be attributed to the C-C(O)-C of the non conjugated ester group.

The dimerization has a strong influence on the contribution from the two carbon atoms bound to oxygen in the ester chain: when the ester chains point into the same direction (ccp and ttp), the interaction between these chemical groups is strong enough to split the peak at the highest wave number (1700 cm^{-1} for the tta' and the cta and at 2000 cm^{-1} for the ccp, ttp and the cca) by about 50 cm^{-1}. This peak (due to the C=O double bond) lies at considerably higher wave numbers (at around 2000 cm^{-1}) for the the ccp, cca and the ttp dimers. What is more, these three dimers show large intensities at particularly low energies (around 1000 cm^{-1}), at odds with the experiment where the center of a broad set of peaks lies higher at around 1200 cm^{-1}. This disqualifies the ccp, cca and ttp dimers since they are not compatible with the experimental spectrum shown in **Fig. 8 (blue line)**. It also indicates that the sample material does not entail the associated interaction.

The geometry of the tta'-dimer, on the other hand, is especially spacious. The ester-chains are distant i.e. partitioned over both sides of the square built by the stereocenters. This lowers the frequency of the highest peak to 1700 cm^{-1} in agreement with experiment (**Fig. 8**). It is interesting to note that the cta dimer (**Fig. 6**, lower panel) shows comparable IR characteristics as the tta' and therefore cannot be ruled out.

We also simulated the linear crosslinked configuration (L-cross in **Fig. 1**). Large contributions from collective vibrations of extended parts of the molecule between 1100 cm^{-1} and 1120 cm^{-1} are observed in the calculated IR spectrum (see supporting material). Additionally, the highest peak is at relatively low wave number (1700 cm^{-1}) but a bit higher than in the Trans and in Cis. Both features are common with the tta' and the cta dimer. Therefore, in IR the distinction between dimerization and crosslinking is difficult (at least since the tta' and the cta dimers have to be considered).

4.2 Characterization of dimers by NEXAFS

On the side of experiment we have developed a procedure to obtain an almost total yield of dimers from the Trans compound, by appropriate exposure to UV light. Due to the pureness of the sample the crosscheck between experiment and theory is most promising.

We first compare NEXAFS spectra of model molecules and dimers and then compute the corresponding quantities by DFT. In this way the contributions of the different atoms can be assigned, and the signatures of a dimer can be distinguished from those of the isomerized compound.

We calculate the NEXAFS spectra of the dimer as a function of the molecular arrangement. The main interest is to check if the realization of the dimer can be tracked in the NEXAFS spectrum. For the dimers considered (ccp, cca, ctp, cta, ttp, ctp', tta') see **Fig. 5**. As the calculated spectra are most reliable in the lowest lying energy region, we focus on the interval between 284 and 286 eV. We check explicitly that the molecular movement at room temperature does not change the peak ordering nor the intensities. **Fig. 9** and supplementary material present

the calculated spectra of these molecules. The experiment (**Fig. 10(f)**) shows an asymmetry of the peak at 285 eV. This can be wrapped with two Gaussian peaks separated by 0.4 eV and an intensity ratio of 3:2. The calculated spectra containing two Cis isomers (cca and ccp, **Fig. 9 c) and d)**) show a symmetric repartition of the shoulder-peaks around the main peak, in disagreement with experiment, so a pure cis-cis cycloaddition can be ruled out. The spectra from trans-trans dimers (parallel or antiparallel, **Fig. 9 a) and b)**) agree with experiment. Combinations of Cis and Trans (as well as the trans-cis diastereo isomers that are not shown), give symmetric shoulder peaks for the ctp' dimers while the ctp and the cta dimers (**Fig. 9 d and e)**) have asymmetric right shoulder peaks as in the experiment (**Fig. 9 f**).

The assignment of the lowest energy NEXAFS peaks to atomic contributions confirms that the origin of the lowest lying peaks is from aromatic rings.

5. ^{1}H NMR spectroscopy

The chemical structures of the compounds Trans, Cis and Dimer have been investigated by ^{1}H NMR spectroscopy in DMSO-D6 (deuterated dimethylsulfoxyde). **Fig. 10** shows the spectra of the three model compounds. They display spectral characteristics consistent with its assigned structure. Indeed, the structures of the Trans and Cis were unambiguously confirmed by the presence of the two characteristic signals of the double bond protons of the cinnamate unit at 6.38, 7.55 ppm and 6.85, 5.76 ppm respectively. The vinylic signals of the Cis are upfield by about 0.4 ppm from Trans. A difference between their coupling constant is also significant and lead to distinguish both isomers., i.e. 15.9 Hz and 12.9 Hz for Trans and Cis respectively. The structure of Dimer was confirmed by the extinction of the signals corresponding to vinylic protons and the presence of two characteristic dd generated by the protons of the cyclobutane

ring at d= 3.76 and 4.20 ppm. We repeated the analysis with C NMR spectroscopy, and we obtained characteristic shifts as before. We then computed NMR spectra using DFT, and we could confirm the abovementioned assignments, and demonstrate in particular the possibility to detect the dimer configuration from a linear crosslinked one, a strength of the method of particular relevance for polymer film application. The comparison between experiment and theory in the ^{1}H case is summarized in **Figure 10**.

6. Discussion

Each of the experimental and theoretical methods applied in this paper addresses different properties of the studied systems, and the combination of such techniques builds up an effective strategy of characterization.

As we have shown, the NEXAFS at the carbon K-edge has proven to be especially sensitive to the delocalized π-states on phenyl rings and the hybridized states in the C=C double bond. At higher energies the interpretation of the NEXAFS is not straightforward due to the short lifetime of the excited (mostly σ-) states resulting in broad peaks and due to their overlap with the continuum states. The remaining resonances are often not sufficient to fully characterize the material. For example, we observed that several isomers of the dimer had similar NEXAFS signature.

IR can help the characterization, as it is easily accessible and it has good capacities to identify functional groups. Once some structural details are known, IR simulations can be performed. Our calculations show that the IR signature is very sensitive to stereo-isomers and allows the detection of isomers containing several functional groups.

For discriminating the dimers, the combination of IR and NEXAFS allows the exclusion of all but two possibilities (cta and tta'), and the DFT energetics confirms that one of these two configurations (tta'), compatible with both experimental techniques, is indeed the most stable.

NMR spectroscopy completes our study. It can - in general - detect small structural differences. We use it to identify the L-cross signature (see **Fig. 10**, upper right panel). Due to the overlap of some resonances and to some differences between experimental and calculated spectra emerging from doing calculation on molecules in the gas phase the interpretation of NMR spectra alone is not unambiguous. Especially for the distinction of different isomers of the dimer it is safe to combine NMR with complementary methods such as IR or NEXAFS. Finally, we underline the importance of DFT calculations: they provide insight into the molecular structures and can identify the atomic origin of the various contributions in every kind of spectroscopy considered.

7. Conclusions

Summarizing, in this work a strategy including experimental and theoretical analysis based on NEXAFS, IR and NMR spectroscopies has proven to be effective for the identification of reactants and products of the kind that are observed in the typical UV or thermally induced processes of technological relevance for the production of orienting films in the LCD industry. We note that in the case of the model molecule (as shown before) there is a dipole moment oriented along the molecular axis, whereas in the case of the dimer the accumulation of charge on the four oxygen surrounding the cyclobutane group destroy such dipolar feature; we are currently investigating the influence of electrostatics on the width of the peaks in the NEXAFS spectra.

In conclusion, we have developed a coherent strategy for the joint experimental and theoretical analysis of interacting side chains in polymer films of relevance to prealignment applications such as the Rolic photoalignment LCMO process. The use of polarized UV light defines a preferential direction along which a cycloaddition takes place. In the model cinnamate system the cycloaddition corresponds to dimerization. The geometry of the produced dimers can be determined as follows: NEXAFS spectra rule out dimers composed of two Cis molecules, as only the tta' and the cta are in agreement with experiment. The IR experiments also point toward the existence of tta' and cta. Energetically the cta is not favoured (0.44 eV higher in energy than tta'). The crystal structure[30] of cinnamate — consisting of antiparallel oriented molecules in the *a* form here present — would favour an antiparallel linking of molecules, in agreement with all further considerations. Still, the emergence of the tta' dimer configuration as the most stable suggests that antiparallel coupling of Trans molecules can be favoured: this indicates that the interpolymer linking by cycloaddition would be an efficient mechanism for realizing an alignment film. Experimentally, we have found that UV exposed thin films of typical photo-alignment materials, are insoluble in common solvents[31], starting from low exposure doses, which is a strong indication of inter-polymer cross-linking.

The possibility of discerning Cis from Trans isomers in NEXAFS spectroscopy, together with the strikingly different dipolar properties suggests appropriate substitutions enhancing the yield of the cycloaddition reaction and its anisotropy, leading ultimately to advanced photo-alignment materials with the high stability required for the manufacturing of modern LCD panels.

Experimental

Experimental synthesis of molecules. Trans, Cis and dimers of ethyl 4-hydroxycinnamate, (see **Fig. 1**) were chemically isolated with high purity. The synthesis of compound 1 (Trans) is done via esterification of p-coumaric acid. However, the synthesis of compound 2 (Cis-isomer) and compound 3 (Cross-link Dimer) is done by exposing Trans molecules to UV light. The Cis is obtained from exposure of Trans solution to UVA and the Dimer from exposure of thin solid film of Trans to UVA light. Synthesis details of the three compounds are available in supporting information. Unfortunately, attempts to synthesize compound 4 (L-cross), including UV light, were not successful.

Nuclear Magnetic Resonance spectrscopy (NMR). ^{1}H and ^{13}C Nuclear Magnetic Resonance (NMR) spectra were recorded on a Brucker 300 spectrometer.

Fourier transform infrared spectroscopy (FTIR). Sample compounds were coated on Si wafers and dried under vacuum at 50°C for 2 hours. FT-IR spectra were then recorded on an ATI Mattson FT-IR (Genesis Series).

Experimental NEXAFS. Total electron yield (TEY) NEXAFS spectra were recorded via the sample drain current at normal incidence at the PolLux beamline at the Swiss Light Source, Villigen, Switzerland. [32,33] The beamline has an energy resolution (E/DE) of approximately 3000 and linear polarization of approximately 80%. Higher order spectral components are rejected by a higher order suppression mirror system [34].The photon energy dependence of the incident x-ray

beam intensity was measured with a silicon photodiode (AXUVHS5; International Radiation Detectors Inc, California) and used to normalize the spectra. Spectra were measured at multiple areas of each sample (beam size of about 100 microns diameter) in order to check homogeneity.

Atomistic simulation. The electronic and structural properties of model systems representing the molecules in gas phase are investigated by density functional theory (DFT) simulations with the CP2K software package [35].

The ground state DFT electronic structure is obtained within the Gaussian and plane wave (GPW) formalism [36]. In particular, we employ double-zeta-valence polarized basis sets optimized for molecular systems, while the interaction between the valence electrons and the cores is described through Goedecker-Teter-Hutter pseudo-potentials. [37]

The revised PBE scheme [38,39] is used for the representation of the exchange and correlation term, with the additional dispersion correction proposed by Grimme [40] to properly account for the weaker van-der-Waals contributions to the forces.

All the molecules have been first optimized in vacuum, through a Broyden–Fletcher–Goldfarb–Shanno (BFGS) using a convergence criterion for the atomic forces of 10^{-4} Hartree/Bohr. Different properties have been computed on the optimized structures.

For the calculation of IR spectra the same DFT setup (basis-set, pseudopotential, functional) has been used. The power spectrum is simply computed by a vibrational analysis based on a finite-differences procedure, to obtain the force constants. The molecular dipoles are then computed from the centers of the maximally localized Wannier functions, to be able to select the IR active modes and compute the IR spectrum. This procedure makes it also possible to identify the atoms that mostly contribute to specific modes in the spectrum.

The NMR spectra are also obtained from the structures optimized in gas phase. All NMR simulations are based on the all-electron version of the Gaussian and augmented-plane-wave (GAPW) method as implemented in CP2K.

In particular, we apply the density-functional-perturbation-theory approach described in Ref. [41] to compute the induced current density generated by the magnetic field and, consequently, the shielding tensor and the susceptibility. The standard all electron cc-pVTZ basis set is employed for all the elements. In order to be able to compare our results to experimental values, only the isotropic component of the tensor is considered and the chemical shift is computed taking as reference the TMS molecule for both H and C.

Details on the generation of NEXAFS spectra. We use the 6-311++G2d2p basis set for all atoms, which --- in combination with GGA-PBE for the exchange correlation energy --- is proven to give transition energies deviating 1.5 eV at most from experimental values and a good quality of the spectra in a range of about 20 eV above the HOMO.

The carbon K-edge spectrum is computed employing the methodology described in Ref. [42,43] . In a SCF calculation performed for every atom individually, we promote one electron to a virtual orbital to obtain the energy of the first excitation, which corresponds to the K-edge. Also in this case we adopt all-electron calculation to be able to describe the excitation of the core 1s electrons.

All the spectra are computed within the Slater transition potential approximation, employing the half-core hole scheme [44] which is known to reliably reproduce experimental spectra. In order to better align the spectra with the experimental off-set, a rigid energy shift is added which is based on the first core-1a excitation energy as determined from standard D-SCF calculations

(one D-SCF for each excited carbon) [42] The spectra are normalized by setting the total intensity to 1 in the energy region of consideration. The calculated spectra consist of sharp absorption lines. In experiment, these lines are smeared out due to a finite life time of the excited states and due to experimental finesse. In order to compare the calculated results, we apply a well known Gaussian convolution consisting of a line broadening of s=0.48 eV below 295 eV. Between 295 eV and 305 eV the lifetime of the excited states is reduced. We mimic this by increasing s linearly to 8~eV and above 305 eV is set constant to 8 eV[43]

Thermal averaging. To consider the thermal movement, we perform NVT molecular dynamics runs over 15~ps using DFTB, a simplified sampling for the electron-electron interaction allowing to treat large systems[45] . The Nose-Hoover thermostat is used in order to keep the system at room temperature. After equilibration (7.5 ps) we extract 10 uncorrelated atomic configurations. Each snapshot is treated in the following way: First we continue the trajectory for 1 ps within the NVE ensemble and then we calculate the NEXAFS-spectra. Due to statistical sampling, the spectra are subject to an uncertainty that corresponds to an average standard deviation of 0.0008 in average and 0.0035 at its maximum.

Acknowledgements

We acknowledge the Swiss National Supercomputing Centre CSCS in Lugano and Swiss National Science Foundation. D. J. A. acknowledges the financial support of the CCMX analytic platform and of Rolic Technologies. Pollux is funded by the BMBF (project no. 05KS7WE1). The authors thank Mr Blagoj Sarafimov for technical assistance. Supporting Information is available online from Wiley InterScience or from the author.

Received: ((will be filled in by the editorial staff))

Revised: ((will be filled in by the editorial staff))

Published online: ((will be filled in by the editorial staff))

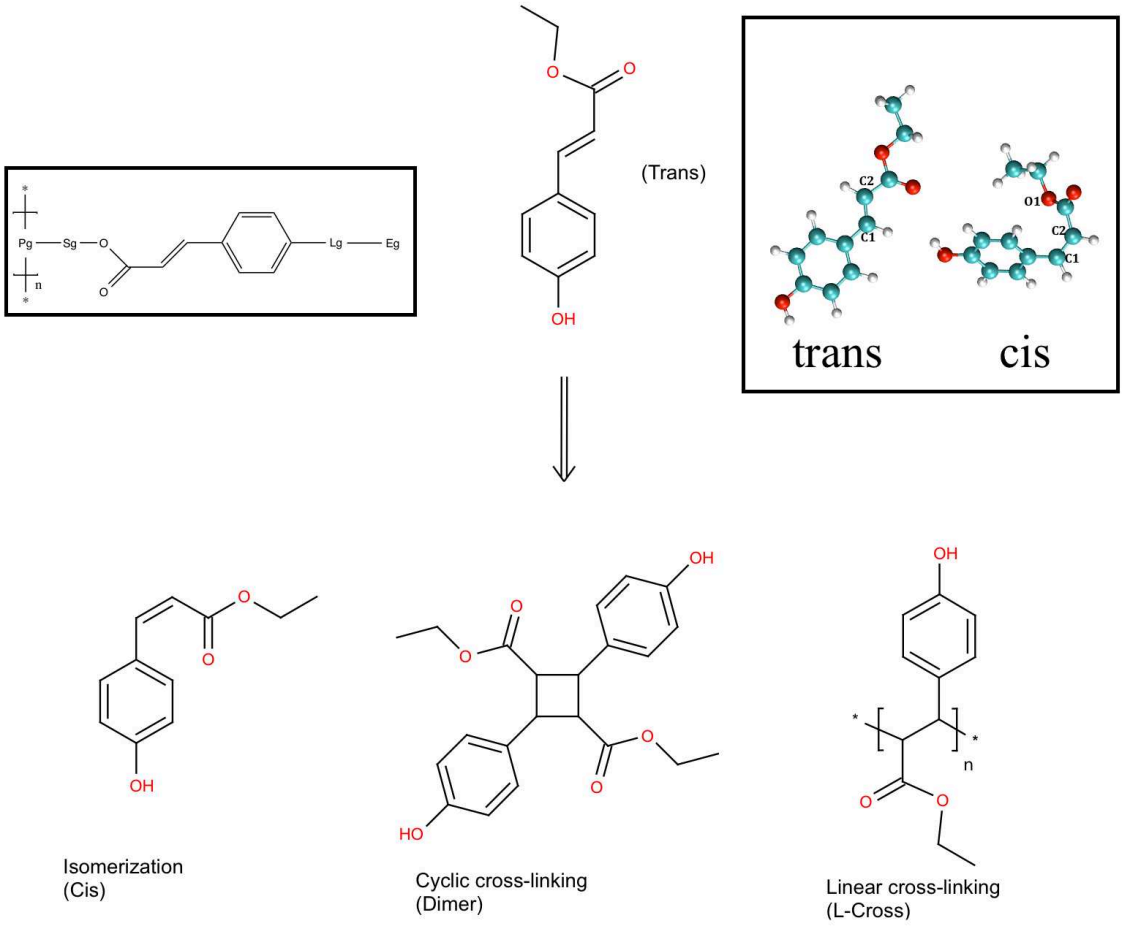

Figure 1. Main possible reaction products after exposure of ethly 4-hydroxycinnamate (Trans) to UV light or thermal treatment: cis-isomerisation (Cis) and 2+2 cycloaddition (Dimer) and linear crosslinking (L-Cross). Insets: Left: Base molecular structure of typical polymers used in commercial products. The polymers consist of a backbone, generally of acrylate or polyimide type, and a side-chain chromophore comprising a cinnamic acid photoactive group linked on both sides to different groups one side, via a linker (Lg), to an end group (Eg) and on the other side to a polymerisable group (Pg), via a spacer (Sg) (adapted from [31]); Right: molecular model of the Trans and Cis configuration, in their optimal geometry.

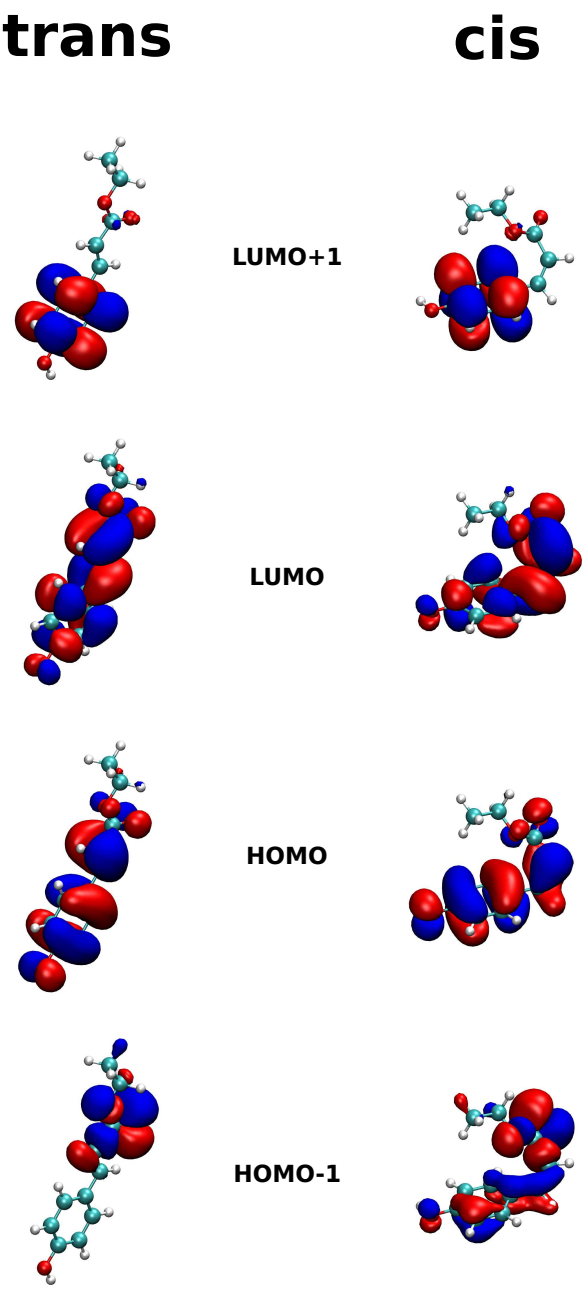

Figure 2. Frontier orbitals for the Trans (left) and Cis (right) isomers.

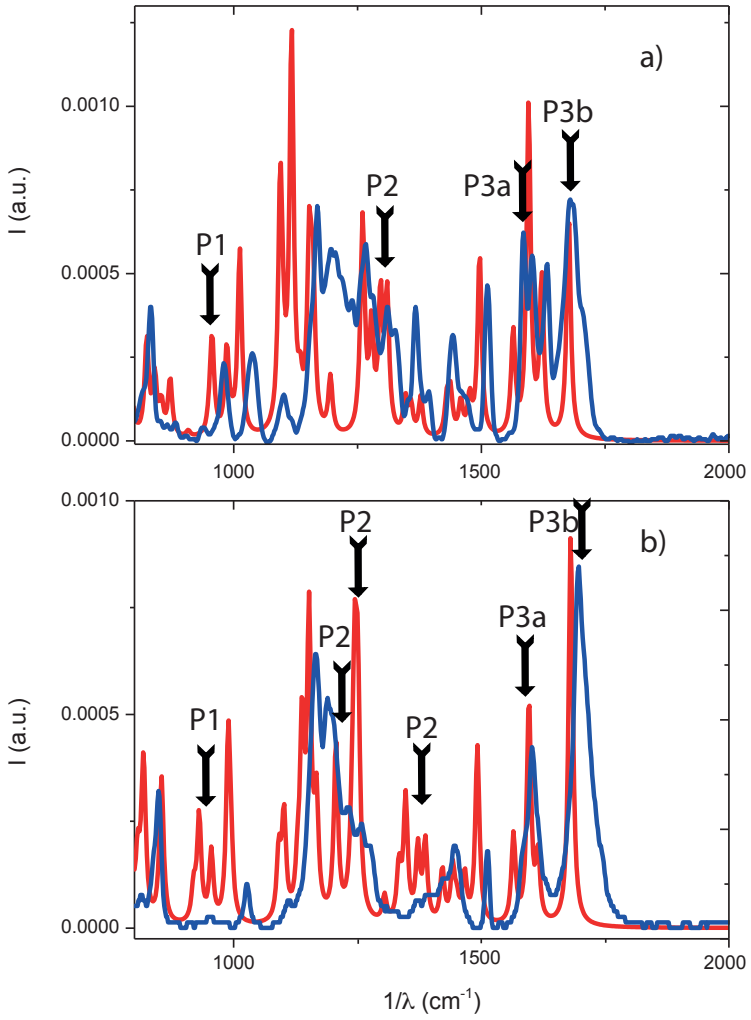

Figure 3. Comparison of the IR spectrum of the Trans (panel a)) and Cis (panel b)) cinnamate. The blue line is the experimental IR-spectrum and the red one is the calculated total spectrum. The shift of the peaks highlighted with letters P1, P2, P3a, P3b is discussed in the text.

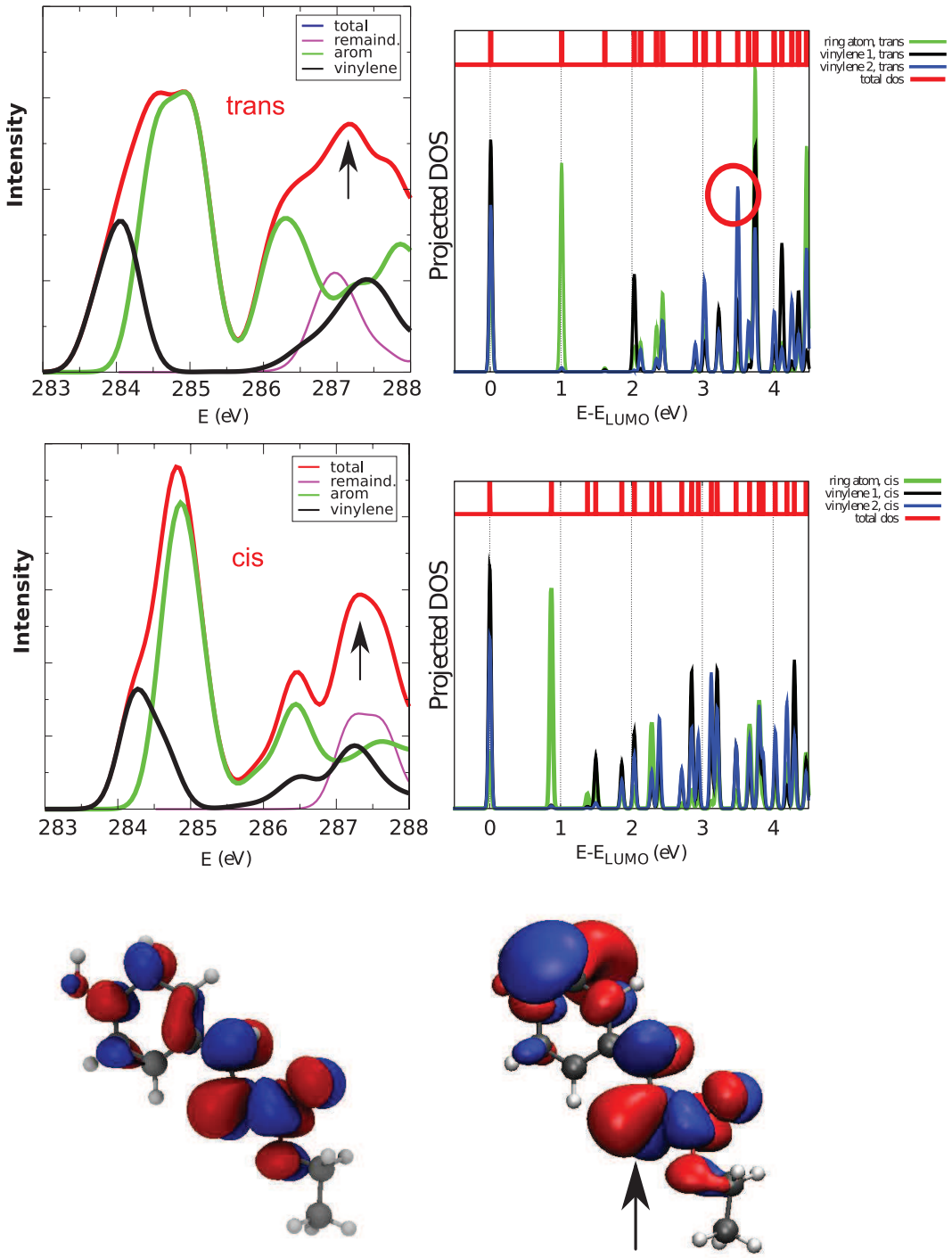

Figure 4. Left panel: theoretical NEXAFS spectrum for the Trans and Cis isomer of the cinnamate. The projections on different molecular components are also drawn. The arrows indicate the peak structure discussed in the text. Right panel: atom projected DOS of the all-electron ground state. The red ellipse indicates the state of the Trans molecule that is not present

in the Cis configuration, which reflects in a higher projection on the vinylene group. Lower panel: representation of the delocalized Trans orbital indicated by the red eclipse (left) and its modification upon exciting an 1s core electron in the vinylene C atom indicated by an arrow (right). This orbital is typical of the Trans configuration.

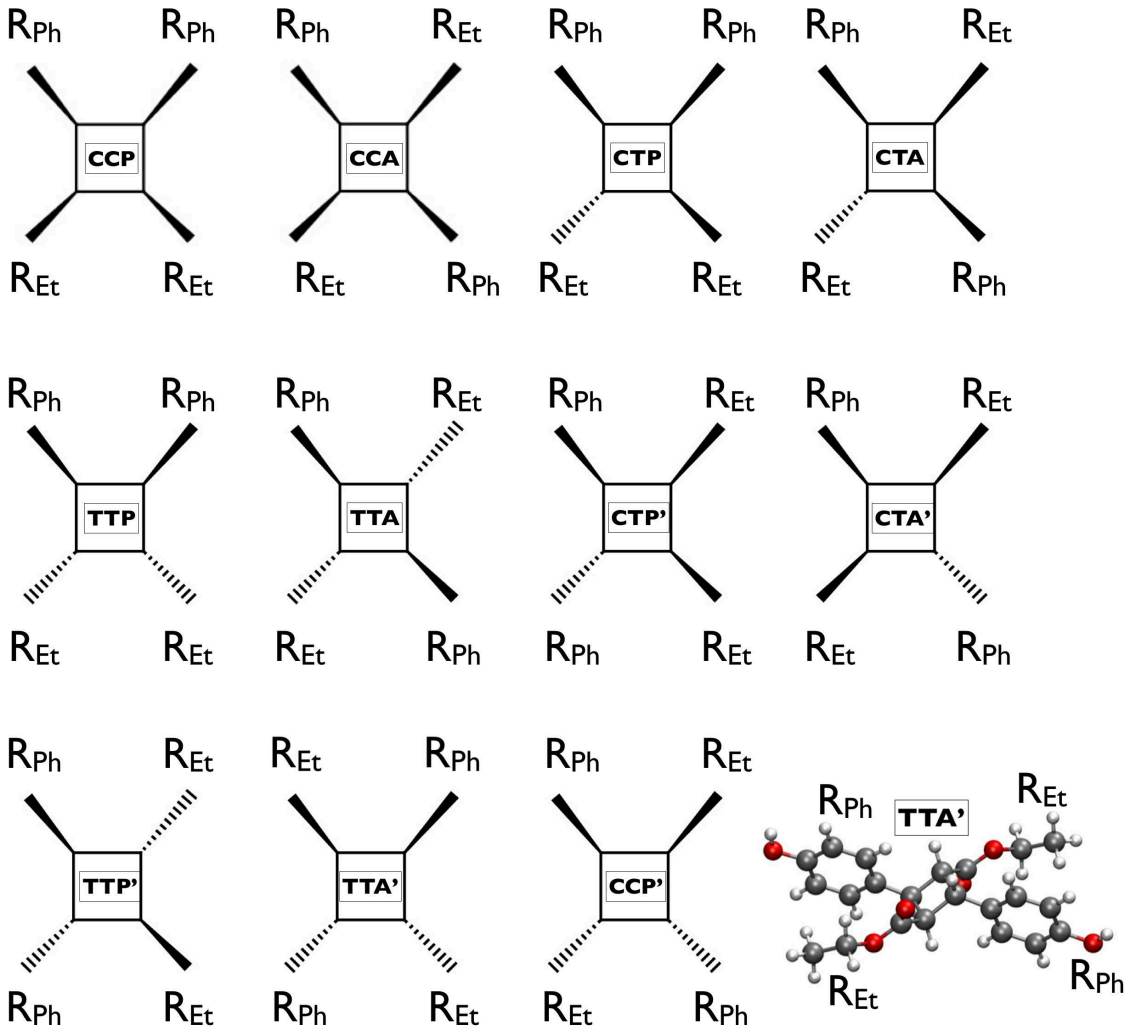

Figure 5. Exhaustive list of all configurations to build a dimer out of two model molecules (trans or cis). The stereochemistry of the subunits containing the phenyl rings (R_{Ph}) and the ethyl

groups (R_{Et}) are evidenced around the central cyclobutane. The molecular model of the TTA' dimer is shown as an example on the bottom right corner.

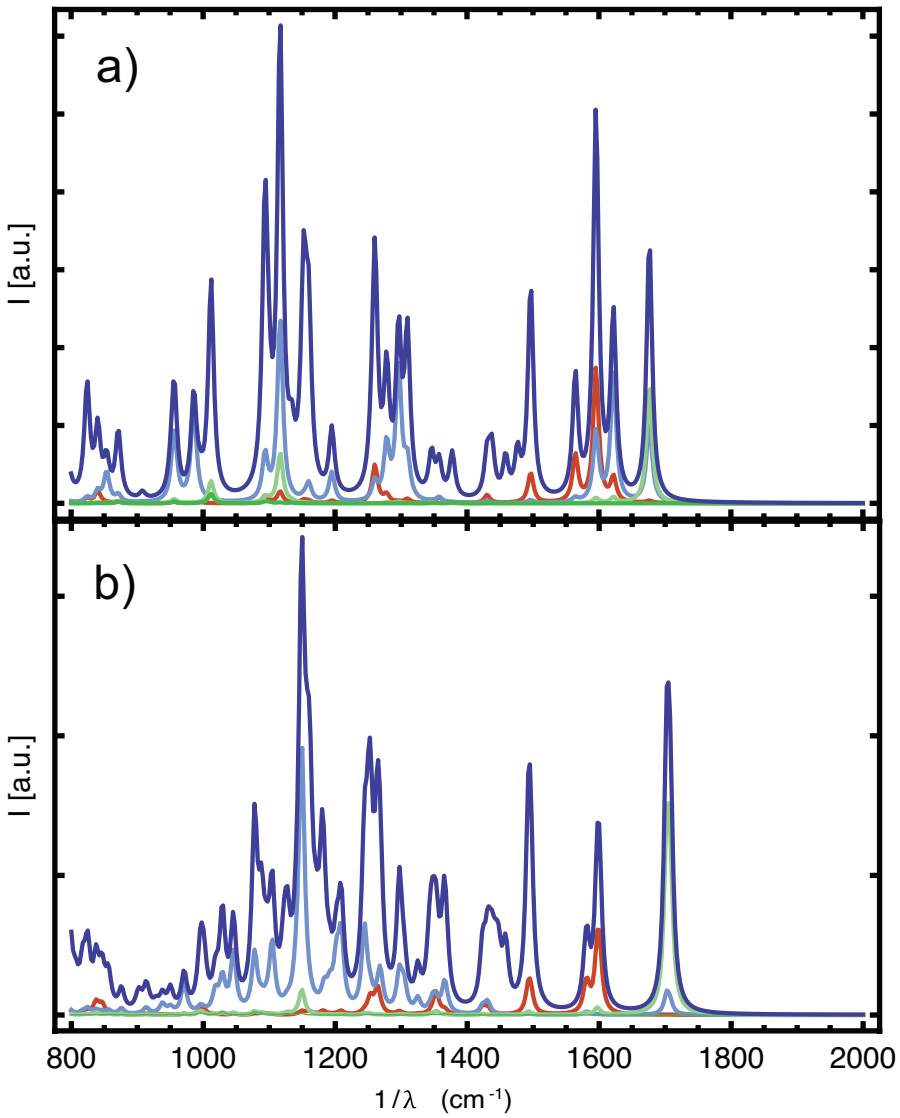

Figure 6. Comparison of the calculated IR spectrum of *trans*-cinnamate (a) and the cta dimer (b). Dark blue is the total IR-spectrum. The further colors are projections of hte vibrational modes on chemical subunits of the molecule rescaled with the IR intensity of the mode: aromatic ring (red), vinylene (top, light blue) or cyclobutane (bottom, light blue), CO (light green) and methyl (dark green). The shift of the peaks of these subunits is discussed in the text.

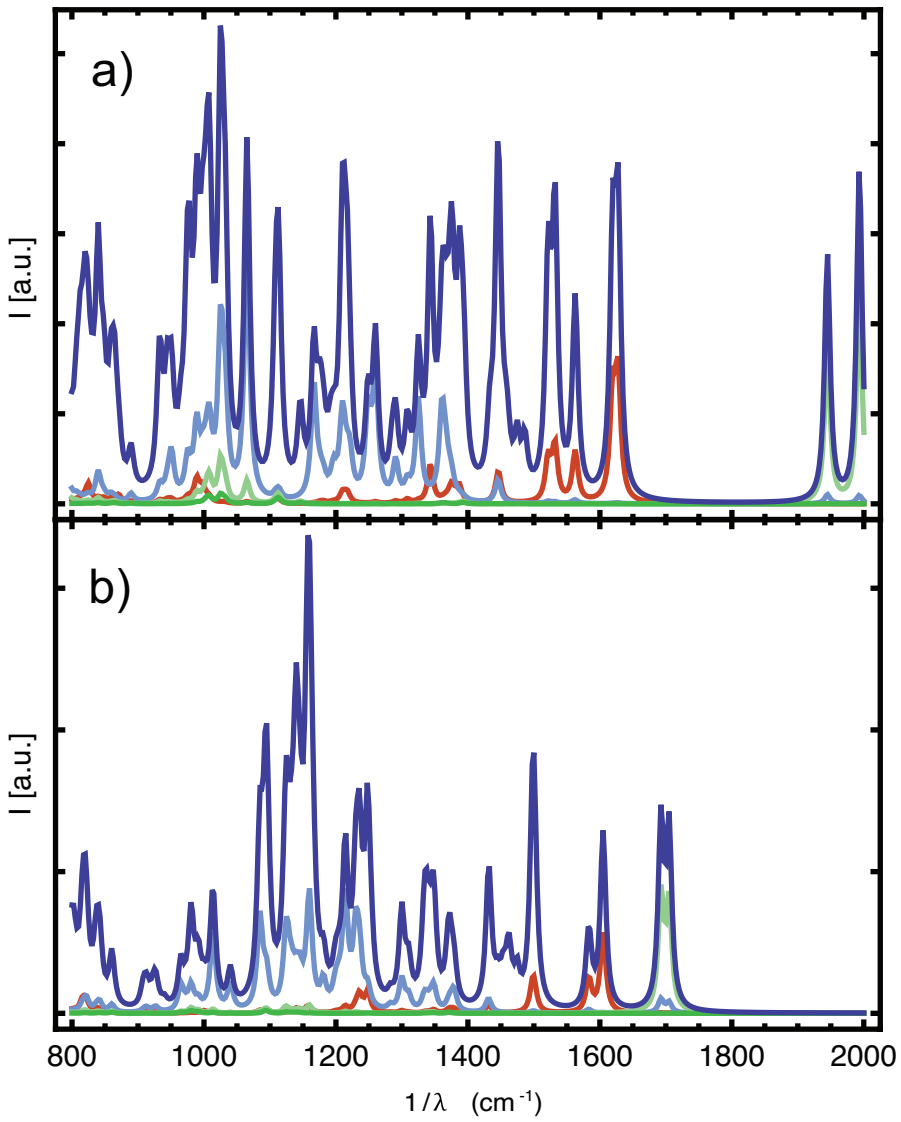

Figure 7: Comparison of the calculated IR spectrum of two different dimers of cinnamate (dark blue), projected on different atomic group contributions: aromatic ring (red), cyclobutane (light blue), CO (light green) and methyl (dark green). In the tta' case (b) a peak at 1700 cm^{-1} that is compatible with the experiment, which is not the case for the ttp case (a).

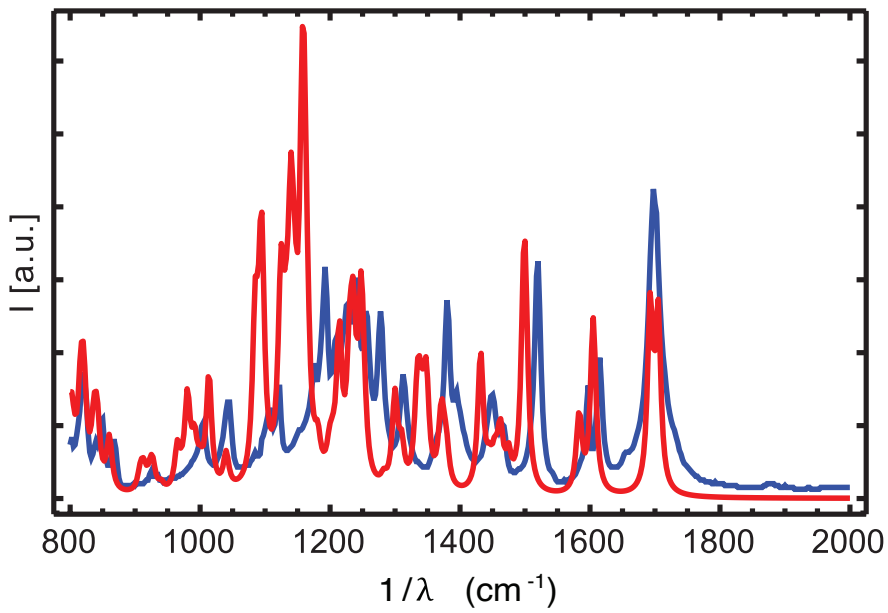

Figure 8. Comparison of the IR calculated spectrum of the tta'-dimer (red) and the measured spectrum of the dimer (blue). Note the experimental peak at 1700 cm^{-1}, reproduced only by two among the stereoisomers in the calculation. Furthermore, the calculations are performed on isolated molecules, whereas in experiment the molecules interact, amongst others through hydrogen bonds. This affects in particular the eigenmodes between 1100 and 1200 cm^{-1}, which involve C-C(O)-C stretching vibration of the ester group.

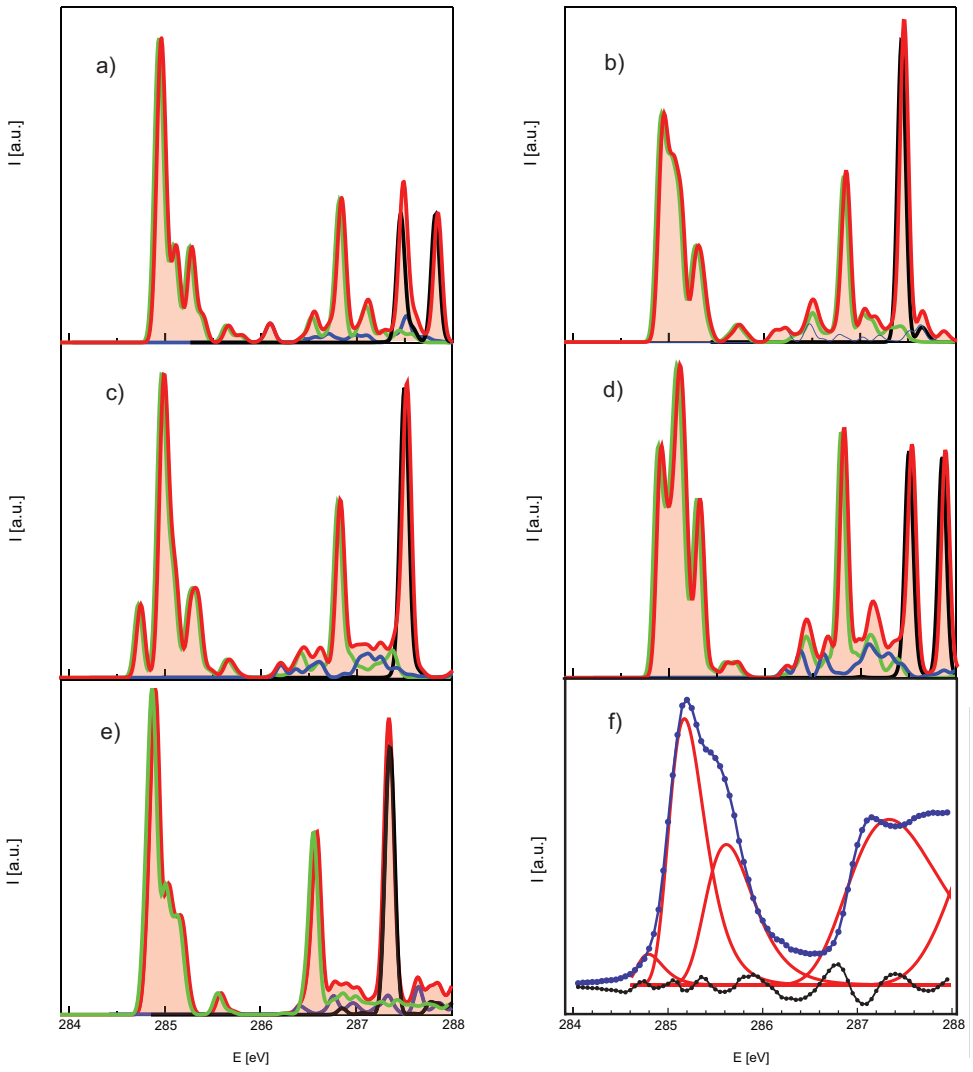

Figure 9. The calculated NEXAFS spectra of the most important realizations of the dimer (red) and the assignment to the contributions of different subunits of the molecule. The peaks in the pre-edge region originate from the phenyl groups. A smaller smearing (s=0.1 eV) has been applied, in order to accent the structure of the pre-peak (panels correspond to dimers: a) tta'; b) ttp; c) cca; d) ccp; e) cta; f) the experimental NEXAFS spectrum of the dimer (blue dots), the decomposition into gaussian contributions (red) and the difference between the two (black dots).

.

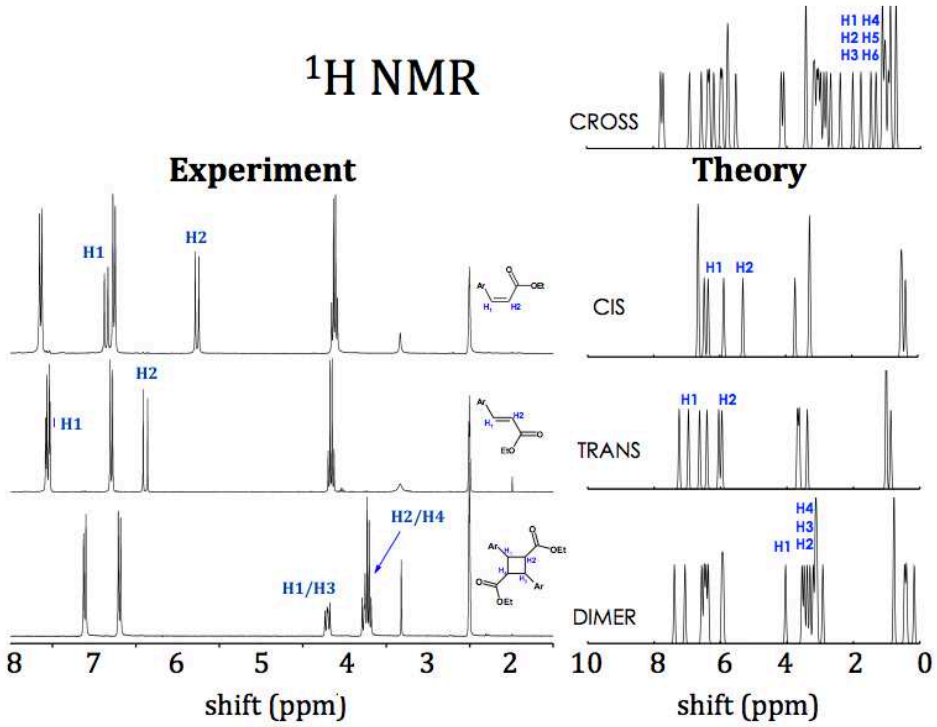

Figure 10. Comparison of experiment (left) and theory (right) in ^{1}H-NMR spectroscopy. Note that the L-Cross spectrum is only available from DFT simulations (upper right panel).

Table 1. Experimental and theoretical IR peaks for the Trans and Cis model molecules (values in cm^{-1}).

		Exp	Theory	Exp	Theory	Exp	Theory
Peak #	Group	Trans		Cis		SHIFT	
P1	C=C	979	986	-	955	-	-31
P2	C=C	1312	1296	1397	1387 (1207/1240)	+85	+91
P3a	C=C	1632	1622	1685	1680	+53	+58
P3b	Conj. C=O	1684	1675	1695	1680	+11	+5

ASSOCIATED CONTENT

Supporting Information. Additional computed properties available as supporting information. This material is available free of charge via the Internet at http://pubs.acs.org

AUTHOR INFORMATION

Corresponding Author

Mohammed Ibn-Elhaj, mohammed.ibnelhaj@rolic.ch

Daniele Passerone, daniele.passerone@empa.ch

Present Addresses

†Present Address: DECTRIS Ltd, Neuenhoferstrasse 107, Baden (Switzerland).

Author Contributions

The manuscript was written through contributions of all authors. All authors have given approval to the final version of the manuscript.

Funding Sources

Any funds used to support the research of the manuscript should be placed here (per journal style).

REFERENCES

(1) K. Miyachi, K.; Kobayashi, K.; Yamada, Y.; S. Mizushima, S. The World's First Photo Alignment LCD Technology Applied to Generation Ten Factor. *SID 10 DIGEST* **2010**, *41,* 579-582.

(2) Eich, M.; Wendorff, J. H. Erasable Holograms in Polymeric Liquid Crystals. *Makromol. Chem., Rapid Commun*. **1987**, *8*, 467–471.

(3) Todorov, T.; Nikolova, L.; Tomova, N. Polarization Holography. 1: A New High-Efficiency Organic Material with Reversible Photoinduced Birefringence. *Appl. Opt*. **1984**, *23*, 4309–4312.

(4) Ichimura, K.; Seki, T.; Hosokit, A.; Aoki, K. Reversible Change in Alignment Mode of Nematic Liquid Crystals Regulated Photochemically by "Command Surfaces" Modified with an Azobenzene Monolayer. **1988**, *1216*, 1214–1216.

(5) Gibbons, W.; Shannon, P.; Sun, S.; Swetlin, B. Surface-Mediated Alignment of Nematic Liquid Crystals with Polarized Laser Light. *Nature* **1991**, *351*, 49–50.

(6) Hasegawa, M.; Taira, Y. Nematic Homogeneous Photo Alignment by Polyimide Exposure to Linearly Polarized Uv. *J. Photopolym. Sci*. **1995**, *8*, 241–248.

(7) Schadt, M.; Schmitt, K.; Kozinkov, V.; Chigrinov, V. Surface-Induced Parallel Alignment of Liquid Crystals by Linearly Polymerized Photopolymers. *Jpn. J. Appl. Phys*. **1992**, *31*, 2155–2164.

(8) Iimura, Y.; Kusano, J.; Kobayashi, S.; Aoyagi, Y.; Sugano, T. Alignment Control of a Liquid Crystal on a Photosensitive Polyvinylalcohol Film. *Jpn. J. Appl. Phys*. **1993**, *32*, L93–L96.

(9) Lu, J.; Deshpande, S. V.; Gulari, E.; Kanicki, J.; Warren, W. L. Ultraviolet Light Induced Changes in Polyimide Liquid-Crystal Alignment Films. *J. Appl. Phys*. **1996**, *80*, 5028–5034.

(10) M. Schadt M.; Seiberle, H. *SID 97 DIGEST*, **397** (1997).

(11) Schadt, M.; Seiberle, H.; Schuster, A. Optical Patterning of Multi-Domain Liquid-Crystal Displays with Wide Viewing Angles. *Nature* **1996**, *381*, 212–215

(12) Schadt, M.; Seiberle, H.; Schuster, A.; Kelly, S. Photo-Generation of Linearly Polymerized Liquid Crystal Aligning Layers Comprising Novel, Integrated Optically Patterned Retarders and Color Filters. *Jpn. J. Appl. Phys* **1995**, *34*, 3240–3249.

(13) Seiberle, H.; Schadt, M. Photoalignment and Photo-Patterning of Planar and Homeotropic Liquid-Crystal-Display Configurations. *J. Soc. Inf. Disp*. **2000**, *8*, 67–71.

(14) Ibn-Elhaj, M.; Schadt, M. Optical Polymer Thin Films with Isotropic and Anisotropic Nano-Corrugated Surface Topologies. **2001**, *410*, 796–799.

(15) Seiberle, H.; Bachels, T.; Benecke, C.; Ibn-Elhaj, M. Volume Photo-Aligned Retarders. *IEICE Trans. Electron*. **2007**, *E90-C*, 2088–2093.

(16) Yamada, Y.; Sakurai, T.; Miyachi, K. Advanced Technologies for Vertical Alignment Liquid Crystal Display, **2011**, *SID-ME Spring Meeting*.

(17) Egerton, P. L.; Hyde, E. M.; Trigg, J.; Payne, A.; Beynon, P.; Mijovic, M. V; Reiser, A. Photocycloaddition in Liquid Ethyl Cinnamate and in Ethyl Cinnamate Glasses . The Photoreaction as a Probe into the Micromorphology of the Solid. *J. Am. Chem. Soc*. **2000**, *111*, 3859–3863.

(18) Schmidt, G. M. J. Photodimerization in the Solid State. *Pure Appl. Chem*. **2009**, *27*, 647–678.

(19) Egerton, P.; Pitts, E.; Reiser, A. Photocycloaddition in Solid Poly (Vinyl Cinnamate). The Photoreactive Polymer Matrix as an Ensemble of Chromophore Sites. *Macromolecules* **1981**, *100*, 95–100.

(20) Sung, S.-J.; Cho, K.-Y.; Hah, H.; Lee, J.; Shim, H.-K.; Park, J.-K. Two Different Reaction Mechanisms of Cinnamate Side Groups Attached to the Various Polymer Backbones. *Polymer* **2006**, *47*, 2314–2321.

(21) VandeVondele, J.; Krack, M.; Mohamed, F.; Parrinello, M.; Chassaing, T.; Hutter, J. QUICKSTEP: Fast and Accurate Density Functional Calculations Using a Mixed Gaussian and Plane Waves Approach. *Comput. Phys. Commun.* **2005**, *167*, 103–128.

(22) Chae, B.; Lee, S. W.; Ree, M.; Jung, Y. M.; Kim, S. Bin. Photoreaction and Molecular Reorientation in a Nanoscaled Film of Poly(methyl 4-(methacryloyloxy)cinnamate) Studied by Two-Dimensional FTIR and UV Correlation Spectroscopy. *Langmuir* **2003**, *19*, 687–695.

(23) Perny, S.; Barny, P. Le; Delaire, J.; Buffeteau, T.; Sourisseau, C.; Dozov, I.; Forget, S.; Martinot-Lagarde, P. Photoinduced Orientation in Poly(vinylcinnamate) and poly(7-Methacryloyloxycoumarin) Thin Films and the Consequences on Liquid Crystal Alignment. *Liq. Cryst.* **2000**, *27*, 329–340.

(24) NIST Computational Chemistry Comparison and Benchmark Database, NIST Standard Reference Database Number 101, Release 15b, August 2011, Editor: Russell D. Johnson III http://cccbdb.nist.gov/

(25) Krauze-Baranowska, M. Truxillic and Truxinic Acids-Occurrence in Plant Kingdom. *Acta Pol. Pharm.* **2002**, *59*, 403–410.

(26) Dhez, O.; Ade, H.; Urquhart, S. G. Calibrated NEXAFS Spectra of Some Common Polymers. **2003**, *128*, 85–96.

(27) Berg, U. In *The Chemistry of Cyclobutanes*; John Wiley & Sons, Ltd: **2006**, p 83.

(28) Turro, N.; Ramamurthy, V.; Scaiano, J. *Principles of Molecular Photochemistry: An Introduction*; University Science Books, **2009**.

(29) Perny, S.; Le Barny, P.; Delaire, J.; Buffeteau, T.; Sourisseau, C. Molecular Orientation and Liquid Crystal Alignment Properties of New Cinnamate-Based Photocrosslinkable Polymers. *Liq. Cryst.* **2000**, *27*, 341–348.

(30) Soldatov, D. V; Terekhova, I. S. Supramolecular Chemistry and Crystal Engineering. *J. Struct. Chem.* **2005**, *46*, S1–S8.

(31) Ibn-Elhaj, M.; Chappellet, S.; Lincker, F. Rolic® LCMO Photo Alignment Technology: Mechanism and Application to Large LCD Panels. *Solid State Phenom.* **2011**, *181-182*, 3–13.

(32) Flechsig, U.; Quitmann, C.; Raabe, J.; Böge, M.; Fink, R.; Ade, H. The PolLux Microspectroscopy Beam Line at the Swiss Light Source. *AIP Conf. Proc.* **2007**, *879*, 505–508.

(33) Raabe, J.; Tzvetkov, G.; Flechsig, U.; Böge, M.; Jaggi, A.; Sarafimov, B.; Vernooij, M. G. C.; Huthwelker, T.; Ade, H.; Kilcoyne, D.; et al. PolLux: A New Facility for Soft X-Ray Spectromicroscopy at the Swiss Light Source. *Rev. Sci. Instrum.* **2008**, *79*, 113704.

(34) Frommherz, U.; Raabe, J.; Watts, B.; Stefani, R.; Ellenberger, U.; Garrett, R.; Gentle, I.; Nugent, K.; Wilkins, S. Higher Order Suppressor (HOS) for the PolLux Microspectroscope Beamline at the Swiss Light Source SLS. **2010**, 429–432.

(35) The CP2K Developers Group. http://cp2k.berlios.de/ (**2000–2010**).

(36) Lippert, G.; Hutter, J.; Parrinello, M. A Hybrid Gaussian and Plane Wave Density Functional Scheme. *Mol. Phys.* **1997**, *92*, 477–488.

(37) Goedecker, S.; Teter, M.; Hutter, J. Separable Dual-Space Gaussian Pseudopotentials. *Phys. Rev. B Condens. Matter* **1996**, *54*, 1703–1710.

(38) Perdew, J. P.; Burke, K.; Ernzerhof, M. Generalized Gradient Approximation Made Simple. *Phys. Rev. Lett.* **1996**, *77*, 3865–3868.

(39) Zhang, Y. K.; Yang, W. T. Comment on "Generalized Gradient Approximation Made Simple"; *Phys. Rev. Lett.* **1998**, *80*, 890.

(40) Grimme, S.; Antony, J.; Ehrlich, S.; Krieg, H. A Consistent and Accurate Ab Initio Parametrization of Density Functional Dispersion Correction (DFT-D) for the 94 Elements H-Pu. *J. Chem. Phys.* **2010**, *132*, 154104.

(41) Weber, V. V.; Iannuzzi, M.; Giani, S.; Hutter, J.; Declerck, R.; Waroquier, M. Magnetic Linear Response Properties Calculations with the Gaussian and Augmented-Plane-Wave Method. *J. Chem. Phys.* **2009**, *131*, 14106.

(42) Iannuzzi, M.; Hutter, J. Inner-Shell Spectroscopy by the Gaussian and Augmented Plane Wave Method. *Phys. Chem. Chem. Phys.* **2007**, *9*, 1599–1610.

(43) Iannuzzi, M. X-Ray Absorption Spectra of Hexagonal Ice and Liquid Water by All-Electron Gaussian and Augmented Plane Wave Calculations. *J. Chem. Phys.* **2008**, *128*, 204506.

(44) Nilsson, A.; Ogasawara, H.; Cavalleri, M.; Nordlund, D.; Nyberg, M.; Wernet, P.; Pettersson, L. G. M. The Hydrogen Bond in Ice Probed by Soft X-Ray Spectroscopy and Density Functional Theory. *J. Chem. Phys.* **2005**, *122*.

(45) Elstner, M.; Porezag, D.; Jungnickel, G.; Elsner, J.; Haugk, M.; Frauenheim, T.; Suhai, S.; Seifert, G. Self-Consistent-Charge Density-Functional Tight-Binding Method for Simulations of Complex Materials Properties. *Phys. Rev. B Condens. Matter* **1998**, *58*, 7260–7268.

Table of Contents Graphics: